

# Energy Management Strategy with Regenerative-Breaking Recovery of Mixed Storage Systems for Electric Vehicles

Research paper

Zebiri Fouad<sup>1,\*</sup>, Benhenich Abd Elhak<sup>2</sup>, Deboucha Add Elhakim<sup>3</sup>, Kessal Abdelhalim<sup>1</sup>

<sup>1</sup>ULPMRN Laboratory, Faculty of Sciences & Technology, University Mohammed El Bachir El Ibrahimi of Bordj Bou Arreridj, Algeria.

<sup>2</sup>Faculty of Sciences & Technology, Bordj Bou Arreridj University, Algeria

<sup>3</sup>Laboratory of Applied Sciences, Ecole Nationale Supérieure des Technologies Avancées, Algeria

Received: 29 April, 2024; Accepted: 07 July 2024

**Abstract:** The present paper addresses the energy management (EM) strategy between batteries and ultracapacitors (UCs) in a dual-propulsion urban electric vehicle (EV). The use of two propulsion machines proves advantageous for high-performance EVs facing spatial constraints. Allocating load power requirements among the propulsion machines and energy storage components poses a significant challenge in this design. In this paper, the control strategy presents managing the energy flow between the converters and the two brushless DC motors (BLDCs) motors via the DC link in order to maintain the energy demand of the EV coming from the dynamics of the latter. For this, power control is carried out by a management algorithm. This management is based on the power requested/generated by the two machines (BLDCs), the state of charge of the batteries ( $SOC_{bat}$ ) and the state of charge of the ultracapacitors ( $SOC_{uc}$ ). The bidirectional DC-DC converter is controlled with current to ensure the functioning of the motor or the generator of the vehicle. We also integrate the controls of the DC bus and BLDC. Additionally, the recovered energy during braking is stored in the battery or in the UC depending on the operating conditions.

**Keywords:** electric vehicles • battery • ultracapacitor • energy management • brushless DC motor

## 1. Introduction

Despite the advancements in engine technology, the rising tide of vehicles on the road is drowning out any progress made on pollution, especially for greenhouse gases driving global warming (Li et al., 2019). To meet the challenge of further reducing consumption and emissions, the automotive industry first turned to electric vehicles (EVs) that eliminate on-board combustion and thus no longer produce polluting emissions (Salkuti, 2023).

The big challenges that electric vehicles (EVs) face in the duration of energy storage are charging period, battery expense, driving distance, weight and volume (Sun, et al., 2019). Current battery technology, while advancing, still contributes to limited driving range (Sun et al., 2019; Lemian and Bode, 2022). Moreover, EV performance can also decline over time due to high power fluctuations, particularly during rapid acceleration, significantly impacting both reliability and lifespan (Barré et al., 2013). To address these drawbacks, we need a dependable, supplementary energy source that delivers peak power precisely when needed. Here, supercapacitors, with their impressive longevity, high power density and rapid charging/discharging capabilities, are uniquely positioned as a potential solution (Zhang et al., 2017). Hybrid energy storage systems (HESSs) is the act of combining two or more energy sources in the same system in order to exploit the advantages of each source (Kamrul et al., 2021). The combination of battery and

\* Email: f.zebiri@univ-bba.dz

supercapacitors brings very interesting improvements to the storage system in terms of performance, autonomy and lifespan (Kouchachvili et al., 2018; Lahyani et al., 2020). Moreover, one of the main objectives of HESS in the EVs is regenerative braking recovery, which later serves to store the braking energy in both the SCs and the batteries (Kouchachvili et al., 2018). Recovery systems can selectively apply regenerative braking to specific wheels. By controlling the amount of regenerative braking applied to each wheel, the system can effectively redistribute torque and improve vehicle stability during cornering or challenging road conditions. This torque vectoring capability allows for better traction and handling, resulting in enhanced stability (Sandrini et al., 2022). The development of research focuses on the implementation of advanced energy control and management techniques in order to optimise the performance of storage energy sources (Ming et al., 2014; Shen and Khaligh, 2015).

The energy management (EM) of sources in EVs is today a very prominent area of research. It is the system that manages the flow of electrical energy seamlessly from the sources power to the electricals machines, and hence to the wheels of the vehicle and vice versa (Vodovozov et al., 2021). Based on the energy demand and the DC-DC converters, HESSs can be configured in passive, semi-active or active topologies. In the passive arrangement, there are no power control circuits involved; instead, the energy storage systems (ESSs) are connected to the load in parallel. In the semiactive and active hybrid, only one DC-DC converter in the first and two DC-DC converters in the second are used in the circuit architectures (Kuperman and Aharon, 2011).

In the literature, several control algorithms for energy management systems (EMSs) have been studied for EVs; in fact, some works have focused on two control methods; first is the optimisation-based EM strategy (model predictive, dynamic programming [DP], stochastic DP, genetic algorithm, Meta-Heuristic Methods, particle swarm optimisation and robust control) also known as the off-line method (Jing et al., 2017; Rimpas et al., 2022; Sankarkumar and Natarajan, 2020). The advantage of optimisation-based strategies is their ability to provide precise solutions for managing energy in a hybrid source. These strategies involve minimising a criterion or cost function while considering factors such as autonomy, energy losses, storage life, and energy recovery during braking (Yuan et al., 2022). However, the multitude of variables involved, as well as the permanent need to adapt to the environment and the prior knowledge of the desired power cycle (the vehicle's journey), hinders the direct onboard implementation of these methods (He et al., 2012; Lemian and Bode, 2022). The second type of strategy is rule-based EM (including fuzzy logic, neural network-based, frequency-based, finite-state machine, sliding mode and thermostat approaches), which is also known as the online method (Babu et al., 2020). The main advantages of this method are its simplicity and relative speed of implementation in real time. Furthermore, this strategy does not require knowing the route of the vehicle in advance. However, the main flaw of this method is that it is based on the knowledge of the expert who designed the rules and that it is valid only in this area (Itania and De Bernardinis, 2022).

Ultimately, deterministic rule-based methods are the simplest to implement, evaluate and compare. It is towards these that we orient ourselves for the remainder of the study. From this perspective, we have chosen to work on the following management strategies: the separation of frequency power and battery power limitation.

This paper proposes a novel EM strategy for EVs equipped with a hybrid storage system (lead-acid battery and ultracapacitors [UC]) during regenerative braking. Our strategy aims to optimise the energy recovery by effectively managing power flow between the electric motors/generators and the two storage devices, thereby extending battery life and improving overall vehicle efficiency under braking conditions.

## 2. HESS in EV Description, Modelling and Control

### 2.1. System description

To determine an adequate management strategy, one must know the behaviour of the system according to the input data. This knowledge is achieved through modelling and simulation. The EV will be studied, consisting of two electrical sources (batteries and supercapacitors) and two brushless DC motors (BLDCs) interconnected through power converters.

The essential parts of an EV, as shown in Figure 1, are power sources, electrical machines, power converters and a control system.

### 2.2. Lead-acid battery

The lead-acid battery is the most commonly used technology in EVs due to its low cost and availability (Venugopal and Reka, 2023). The reaction of these batteries is not the same according to the applications and the constraints to

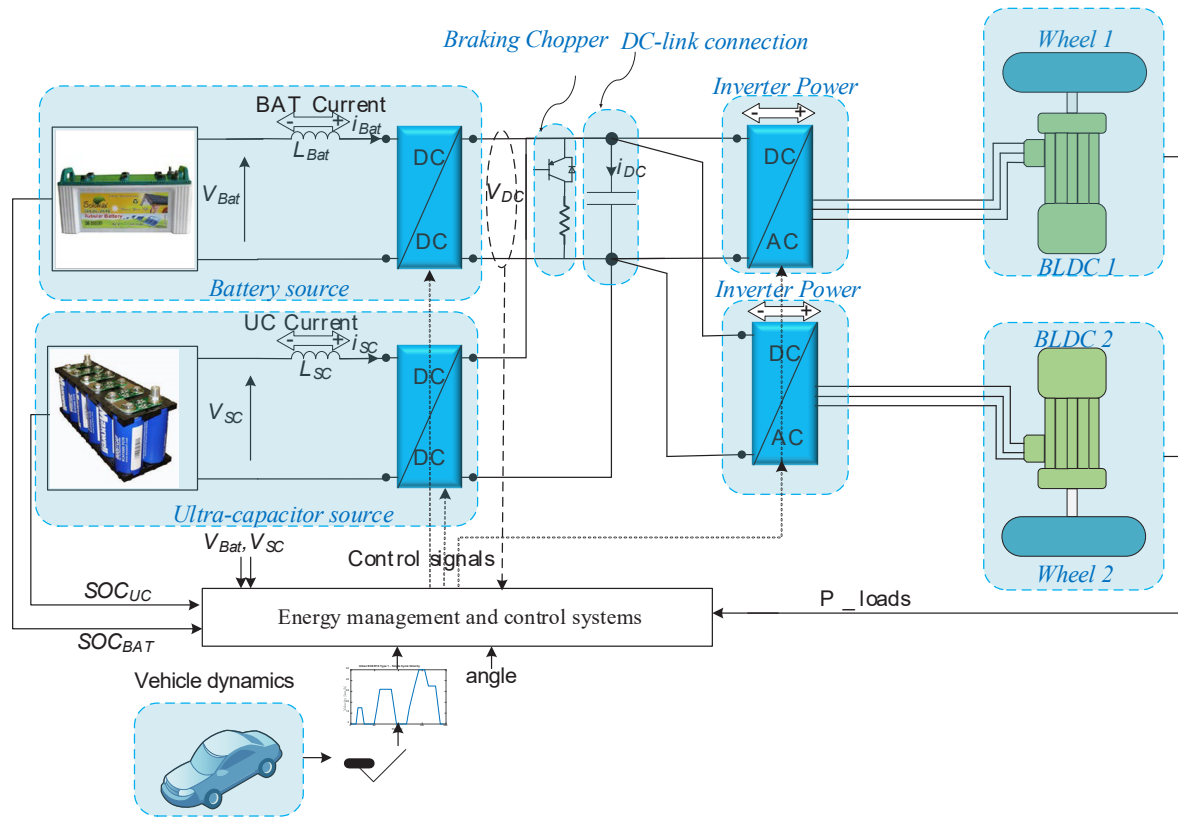


**Figure 1.** Proposed structure for the implementation of the management system. BLDC, brushless DC motor.

which they are subjected, which is why we cannot find a single model for all cases. In the literature, the most widely used models are the simple electric model of a battery, also called the R-C model, and the so-called ‘CIEMAT’ model (Research Center for Energy, Environment, and Technology) (Yahya and Ould Mahmoud, 2007). A typical example of an R-C model is presented in Figure 2.

$$V_{Bat} = n_b (E_{Bat} \pm R_{iBat} I_{Bat}) \begin{cases} E_{Bat} = f(SOC) \\ R_{iBat} = f(I_{Bat}, SOC, T) \end{cases} \quad (1)$$

$E_{Bat}$ , the open circuit voltage at the battery terminals, represents the electromotive force.  $R_{iBat}$ , the internal resistance, whose value depends on the battery’s state of charge (SOC), represents the energy losses within the battery.

The capacitance model gives the amount of energy that can be released depending on the discharge current  $I_{Bat}$ .

### 2.3. UC

When compared to typical electrochemical capacitors, UCs have a high energy density. Recently, their ability to store energy quickly has made them particularly suitable for regenerative braking applications, whereas batteries have difficulty in this application due to slow charging rates. The simplest model is based on the  $R_c$  (Figure 3) charging circuit time constant. However, this model does not consider all the phenomena existing within a supercapacitor (Ma et al., 2023).

### 2.4. DC-DC converters

Two converters are connected via a DC bus whose voltage ( $V_{dc}$ ) gives the overall system more flexibility and expandability. The first converter manages the battery energy flow and the second manages the supercapacitor energy flow. In this case, a bidirectional Buck&Boost DC-DC converter is used (AC and Reddy, 2022). This converter

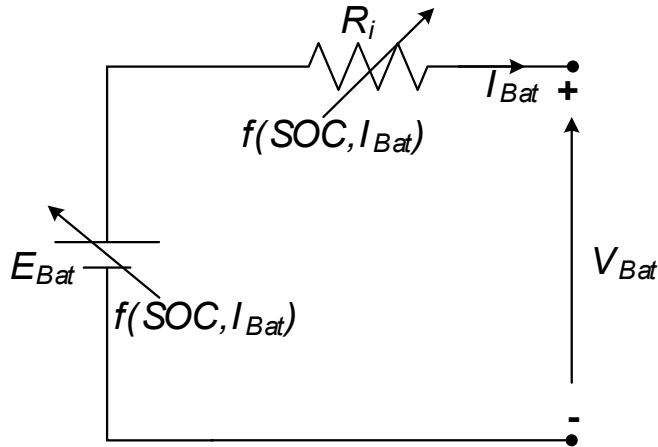


**Figure 2.** The equivalent electrical circuit of the CIEMAT battery model.

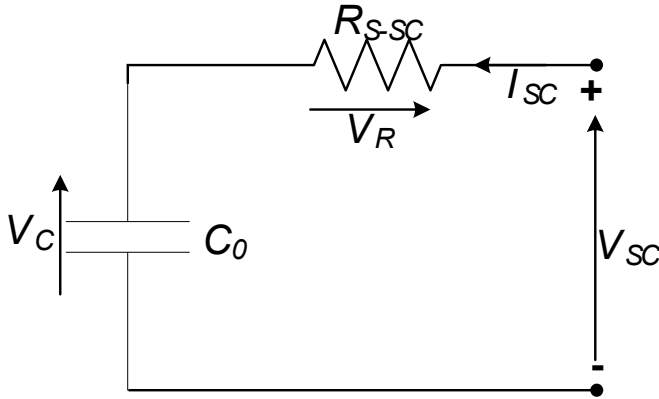


**Figure 3.** The equivalent electrical circuit of UC. UC, ultracapacitor.

operates as Boost if you want to discharge the storage elements and as Buck if you want to charge them. In order to model them, we perform a linearisation around an operating point by considering their average model. This linearisation is justified because the switching frequency ( $f_s = 1/T_s$ ) is large compared to the evolution of the physical quantities of the converters.

### 2.4.1. Averaging modelling

In order to illustrate the modelling of static converters, we consider the converter associated with batteries. The current  $i_{L,Bat}$  and the voltage  $V_{Bat}$  are state variables for this converter.

The duty cycle controlling the converter is denoted ' $\alpha$ ' and it is between 0 and 1.

Figure 4 shows the two switching phases of the IGBTs. By analysing the electrical circuit, we can derive the non-linear average model for our subsystem.

$t \in [0 - \alpha T_s]$  ( $S_{boost}$  is closed)

$$V_{Bat} - L_{Bat} \frac{d}{dt} i_{L,Bat} = 0 \quad (2)$$

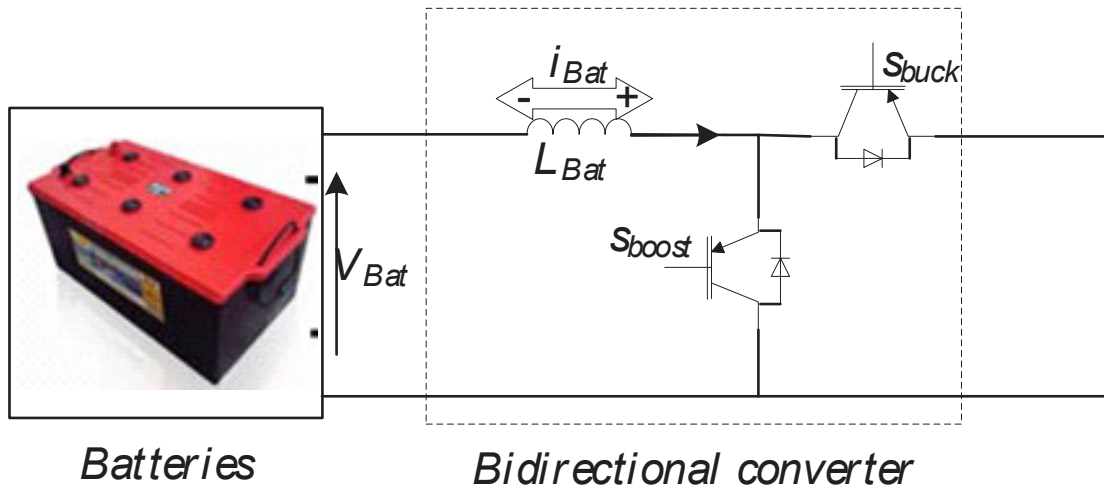


**Figure 4.** Batteries converter.

$t \in [\alpha T_s - T_s]$  ( $S_{boost}$  is open)

$$V_{Bat} - L_{Bat} \frac{d}{dt} i_{L,Bat} - V_{DC} = 0 \quad (3)$$

by combining Eqs (2) and (3),

$$V_{Bat} - L_{Bat} \frac{d}{dt} i_{L,Bat} (1 - S_{Bat}) V_{DC} = 0 \quad (4)$$

The switch state  $S_{Bat}$  corresponds to the closed state when assigned the value '1' and the open state when assigned '0'.

Integrating both sides of Eq. (4) over the switching period ( $T_s$ ) yields the averaged model,

$$V_{Bat} - L_{Bat} \frac{d}{dt} i_{L,Bat} - (1 - \alpha) V_{DC} = 0 \quad (5)$$

We note that: 
$$\int_0^{T_s} S_{Bat} dt = \int_0^{\alpha T_s} 1 dt + \int_{\alpha T_s}^{T_s} 0 dt = \alpha T_s$$

Eq. (5) can be rearranged as follows:

$$\frac{d}{dt} i_{L,Bat} = \frac{1}{L_{Bat}} (V_{Bat} - (1 - S_{Bat}) V_{DC}) \quad (6)$$

$t \in [0, \alpha \cdot T_s]$   $t \in [\alpha \cdot T_s, T_s]$

The dynamic behavior of the static converter can be analyzed using the average model presented in Figure 5.

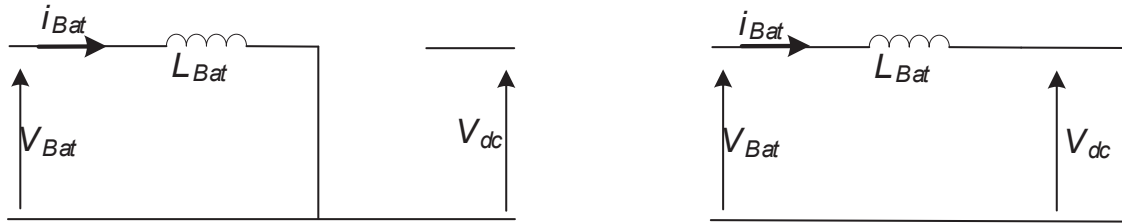


**Figure 5.** Average model of a static converter.

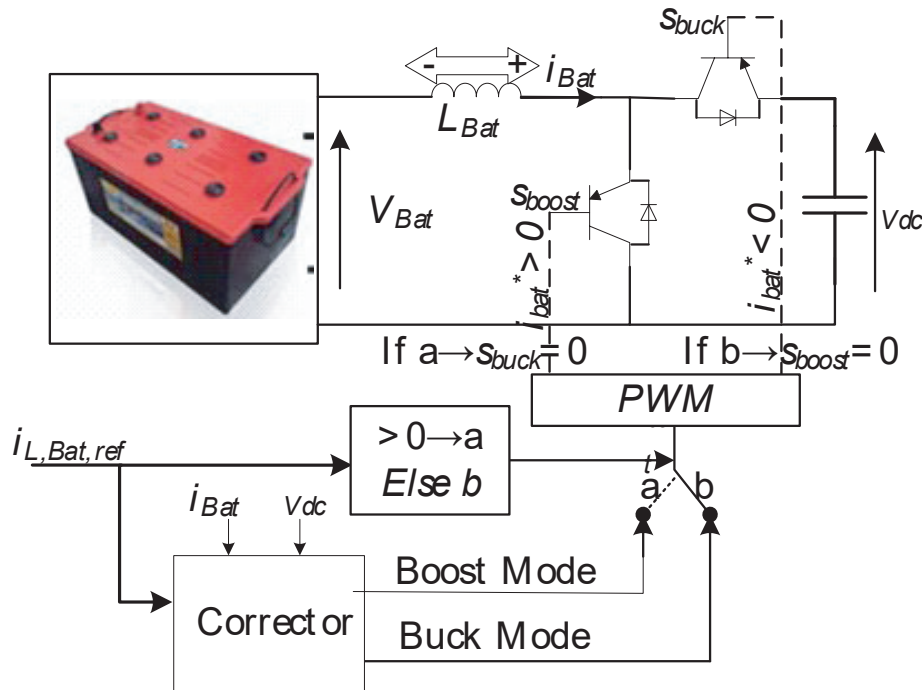


**Figure 6.** The control scheme of the storage converter.

#### 2.4.2. Current control of converters associated with batteries and supercapacitors

Two control laws must be included in the converter control system, the first for the Boost mode and the second for the Buck mode. The control block diagram is shown in Figure 6. The inductor current ( $i_{L,Bat}$ ) is a state space variable within the system.

To manage the flow of energy between various sources and the load, the DC-DC converters employ current control via a PI controller as show in Figure 7.

### 2.5. DC-link voltage regulation

Static converters associated with the batteries and supercapacitors are current-controlled. This allows the management of power flows between the storage elements and the load interconnected via the DC bus. EV motors are speed-controlled, and they constitute the load of the system. Thus, the motor currents ( $i_m$ ) are considered as disturbances.

We therefore propose to control the DC bus voltage using the principle (Paire et al., 2010) described in Figure 8. A PI controller calculates the reference current ( $i_{dc,ref}$ ) in order to maintain the bus voltage at the reference voltage ( $V_{dc,ref} = 300$  V). An EMS develops the current references for the static converters of the batteries and supercapacitors (respectively,  $i_{bat,ref}$  and  $i_{sc,ref}$ ).

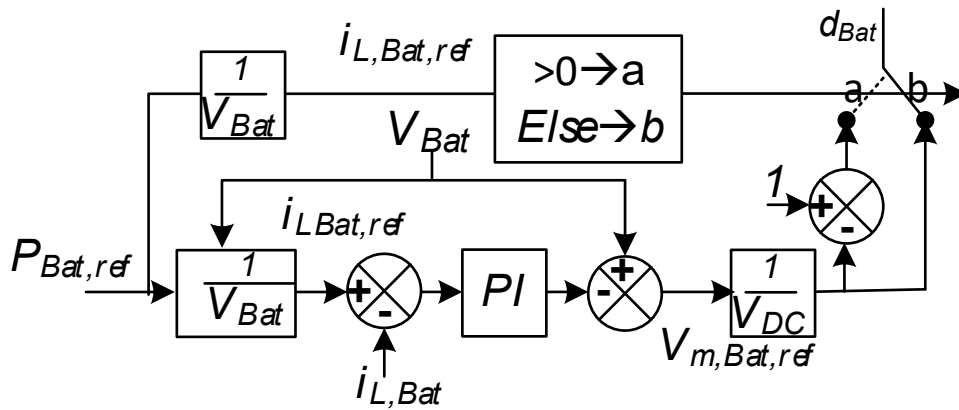


Figure 7. PI control loop of the storage converter.

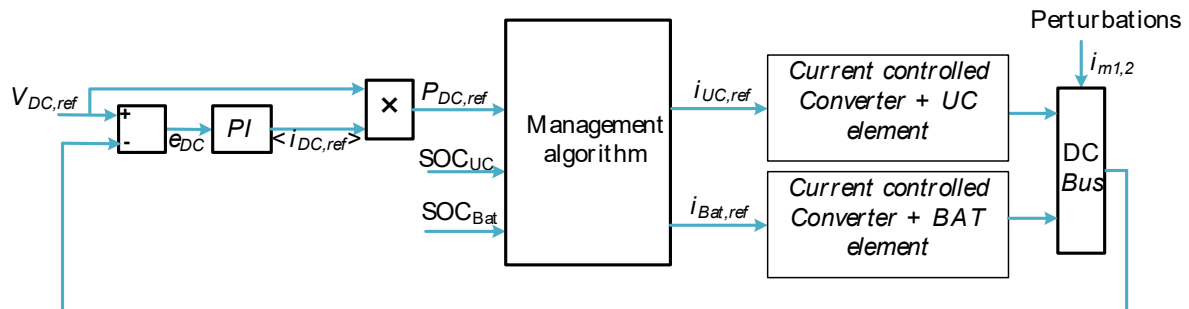


Figure 8. DC-link voltage control loop.

## 2.6. Speed control for BLDC drives

### 2.6.1. BLDC model

An understanding of the dynamics of an electric motor is necessary for understanding the behaviour of the motor. The mathematical equations (electrical and mechanical) and the expressions of the FEMs are exploring in this section. To proceed with the analysis of the BLDC motor, it is essential to establish certain assumptions:

- **Linear Magnetic Circuit:** The magnetic circuit of the machine is assumed to be unsaturated, allowing for the expression of magnetic fluxes as a linear function of phase currents. Magnetic saturation will not be considered in the equations.
- **Stator Coil Symmetry:** The symmetry of the three stator coils is assumed. This implies that the coils have identical electrical and geometrical properties.
- **Trapezoidal Rotor Flux Density:** The distribution of the magnetic flux density generated by the rotor poles is assumed to be trapezoidal. This simplifies the analysis and aligns with the typical design of BLDC motors.
- **Star-Connected Stator:** The three stator phases are assumed to be connected in a star configuration, with the neutral point inaccessible. This is a common connection method for BLDC motors.
- **Negligible Temperature Effect on Resistance:** The impact of temperature variations on the resistance of the stator windings is considered negligible. This assumption is typically valid within the operating range of the motor.
- **Negligible Eddy Currents:** The effects of induced currents, also known as eddy currents, are assumed to be negligible. Eddy currents can arise from the interaction of the changing magnetic fields with the conductive materials of the motor.

### A. Electrical system

The three phase currents for the stator windings of a BLDC motor can be expressed as (Chojowski, 2018):

$$\begin{cases} \frac{di_a}{dt} = \frac{1}{L_s - M}(V_{an} - e_a - Ri_a); \\ \frac{di_b}{dt} = \frac{1}{L_s - M}(V_{bn} - e_b - Ri_b); \\ \frac{di_c}{dt} = \frac{1}{L_s - M}(V_{cn} - e_c - Ri_c); \end{cases} \quad (7)$$

where,  $i_a, i_b, i_c$  (A) represent stator phase currents,  $V_{an}, V_{bn}, V_{cn}$  (V): stator phase voltages,  $e_a, e_b, e_c$  (V): trapezoidal phases back emf,  $R$ : stator resistance per phase;  $L_s$ : stator inductance per phase and  $M$ : mutual inductance.

It is assumed that the winding-induced EMF is trapezoidal and equal to the flux change rate. They are expressed as (Zebiri et al., 2016):

$$\begin{cases} e_a = f_a(\theta_r)\psi_p\Omega_m; \\ e_b = f_b\left(\theta_r - \frac{2\pi}{3}\right)\psi_p\Omega_m; \\ e_c = f_c\left(\theta_r + \frac{2\pi}{3}\right)\psi_p\Omega_m. \end{cases} \quad (8)$$

where,  $\Omega_m$  (rad/sec): mechanical angular velocity;  $\theta_r$ : rotor position (rad); the angle between rotor axis and the axis of phase;  $\psi_p$ : maximum value of BLDC flux linkage of each winding; and  $f(\theta_r)$ : unit function representing the waveform of the back-EMF and  $\theta_r$ .

### B. Mechanical system

The speed and torque of the motor are obtained using the following equations:

$$\begin{cases} \left(\frac{d\Omega_m}{dt}\right) = \frac{1}{J}(-B\Omega_m + T_e - T_L) \\ T_e = \psi_p [i_a f(\theta) + i_b f(\theta - 2\pi/3) + i_c f(\theta + 2\pi/3)] \end{cases} \quad (9)$$

where,  $T_L$ : the load torque,  $B$ : the frictional coefficient and  $J$  is the moment of inertia.

#### 2.6.2. Speed control for BLDCM drives

The BLDC motor is driven by the change in the phase windings. This is achieved by exciting the position of a permanent magnet on the rotor in order to produce a continuous torque (Figure 9) (Sen et al., 2023). This condition is well assured by the control of the BLDC speed using direct current control. The PI controller is the most commonly used in BLDC motor drive systems for speed control. In this section, we will introduce how to design a speed controller, i.e. how to select the P and I gains of a PI speed controller for the desired performance (Zebiri et al., 2022).

The PI controller consists of a proportional term, which depends on the present error, and an integral term, which depends on the accumulation of past and present errors as follows:

$$G_{PI}(S) = K_p + \frac{K_I}{S} \quad (10)$$

where  $K_p$  and  $K_I$  are the proportional and integral gain, respectively.

The closed loop block diagram to the speed with the PI controller is represented in Figure 10.

We can assume the load torque as being a disturbance, because it will be compensated by the integral action (PI controller).

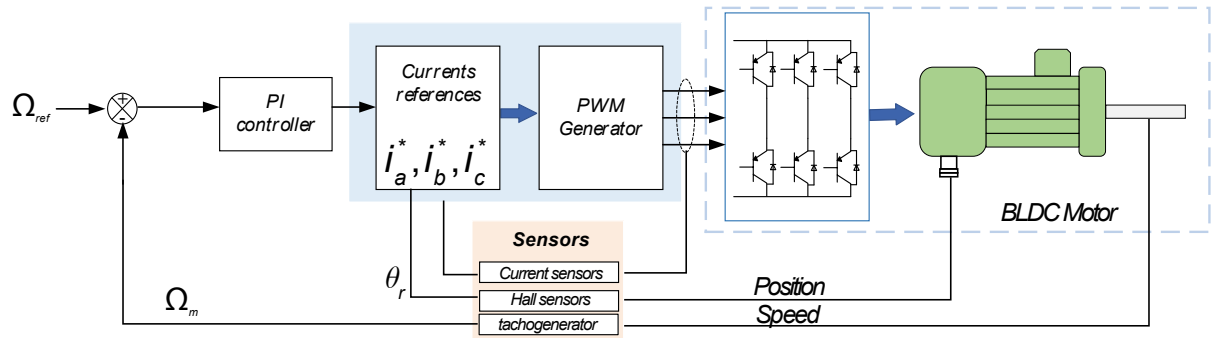


**Figure 9.** The speed-controlled BLDCM drive scheme.

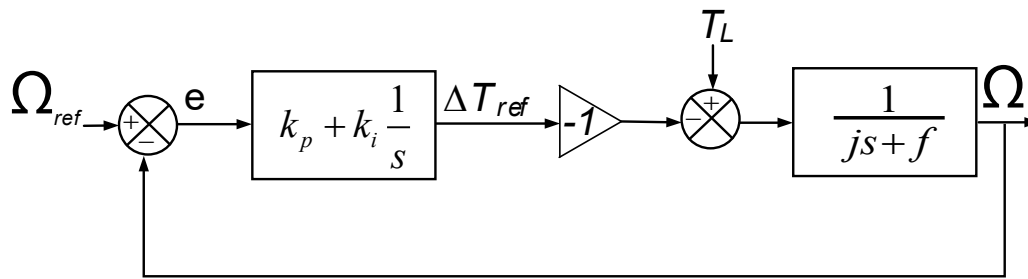


**Figure 10.** Block diagram of the DC motor including a speed controller.

The close loop transfer function is given by Eq. (11)

$$\frac{\Omega_{ref}}{\Omega} = \frac{\frac{1}{J}(K_p s + K_i)}{s^2 + \frac{(K_p + f)}{J}s + \frac{K_i}{J}} \tag{11}$$

The transfer function in Eq. 11 behaves like a second order system; In this case, the P and I gains of the PI speed controller can be designed using the root locus method. The resulting gains are dependent on the desired damping ratio ( $\xi$ ) and undamped natural frequency ( $\omega_n$ ). In this context, we can extract the PI gains of the controller from the second-order transfer function:

$$\begin{cases} K_p = 2J\xi\omega_n - f \\ K_i = J\omega_n^2 \end{cases} \tag{12}$$

We seek for our system a damping ratio to be around to  $\xi = 0.7$ , which we often considered the optimal value for the following two reasons:

- ✓ Closed loop system is stable (the poles of this system lie on the left half plane);
- ✓ low response time.

## 2.7. Vehicle dynamics

The force required to drive the vehicle at the wheels is defined by the equations (Listwan and Oleszczyszyn, 2023):

$$F_T = F_{rool} + F_{aero} + F_{gr} + F_{acc} \tag{13}$$

where,  $F_{roll}$  is the rolling resistance force as a result of the tire flattening at the surface of the road. The second is  $F_{aero}$ , which is called the aerodynamic force. The third is the resistance force due to the slope to be climbed. The fourth represents the dynamic term for vehicle acceleration or deceleration.

$$\begin{cases} F_{roll} \approx MgC_{avr} \\ F_{aero} = 0.5 \cdot \rho \cdot C_x \cdot A_f \cdot (v \pm v_w)^2 \\ F_{gr} = \pm M \cdot g \cdot \sin \alpha_p \\ F_{acc} = \delta \cdot M \frac{dv}{dt} \end{cases} \quad (14)$$

where:  $M$ : the mass of the vehicle,  $v$  (m/s): the vehicle speed,  $v_w$ : wind speed (m/s),  $\alpha_p$  (rad): angle of the slope and  $\delta$  is the rotational inertia factor or mass factor:

$$\delta = 1,04 + 0,0025 \cdot g_r^2 \quad (15)$$

## 2.8. Electronic differential (ED) control of two wheels drive (2WD)

The system under consideration is the Ackermann–Jeantand steering model, with the ED developed so that, on a straight trajectory, the two drive wheels travel at the same speed (Wu et al., 2014). In a curved trajectory, the difference between the two speeds of the wheels determines the speed of the vehicle as the two rear wheels are driven directly by two independent motors (Chhlonh et al., 2021). The structure of the electronic differential is depicted in Figure 11, where BLDC stands for brushless DC motor. The steering model of the vehicle is illustrated in Figure 12, also featuring the BLDC motors.

For the steering angle  $\delta$ , there is a circumstance that can be assumed, where (Chhlonh et al., 2021):

$\delta > 0$  turned right,  $\delta < 0$  turned left and  $\delta = 0$  straight.

The ED instantaneously applies torque adjustments to the two drive motors, compensating for the difference in wheel travel during cornering by decreasing the speed of the inner wheel and increasing the speed of the outer wheel.

In response to the driver's steering input, the ED immediately adjusts the speed of the two motors. It reduces the speed of the inner wheel and increases the speed of the outer wheel to improve handling during cornering. This is illustrated in the block diagram of the ED control system (Figure 13) (Chhlonh et al., 2021; Wu et al., 2014):

$$\begin{aligned} \omega_{r-R} &= \omega_v - \frac{d_w}{2L_w} \tan(\delta) \omega_v \\ \omega_{r-L} &= \omega_v + \frac{d_w}{2L_w} \tan(\delta) \omega_v \end{aligned} \quad (16)$$

Where  $\omega_{r-R}$  is the angular rotating speed at the rear left side,  $\omega_{r-L}$  is the angular rotating speed at the rear right side and  $\omega_v$  is the angular rotating speed at the center of the vehicle.

The speed change between the left and right wheel can be written as:

$$\Delta\omega = \omega_{r-L} - \omega_{r-R} = \frac{d_w}{L_w} \tan(\delta) \omega_v \quad (17)$$

The reference speed of each front wheel:

$$\begin{aligned} \omega_{mR}^* &= K_g \omega_{r-R} \\ \omega_{mL}^* &= K_g \omega_{r-L} \end{aligned} \quad (18)$$

Where:  $\omega_{mR}^*$  and  $\omega_{mL}^*$  are the reference speeds of the two right and left motors, respectively.



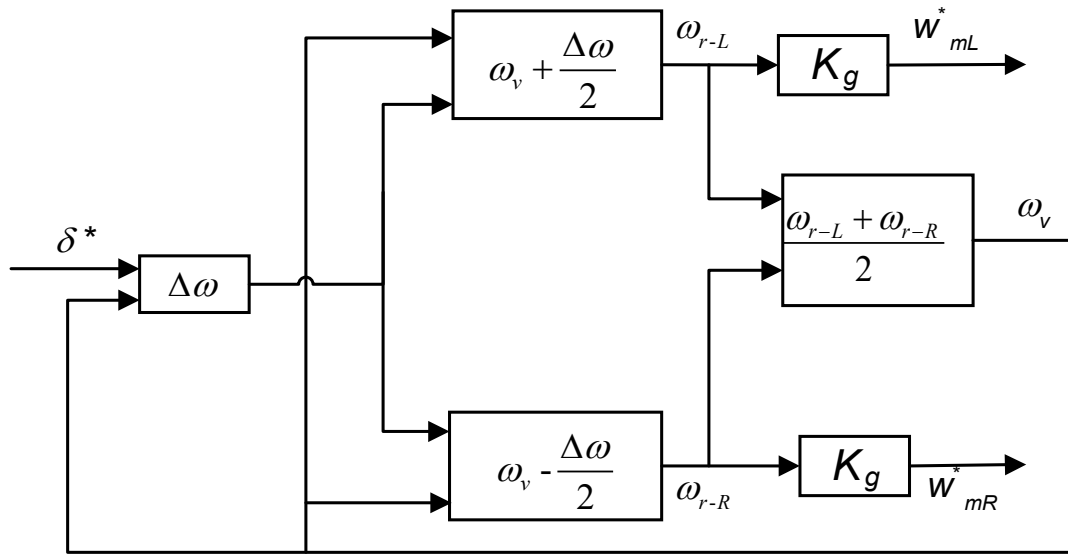


**Figure 13.** The lock diagram of the ED. ED, electronic differential.

### 3. EMS Proposal

Controlling the power flow between various sources is necessary to provide the power needed by the EV. However, a controlled active HESS can recover a greater amount of energy from electric motors (regenerative-braking recovery). Moreover, the electrical energy must be recovered, in priority, by the high-power density storage element, the UC. This is accomplished by the coordinated control of various power electronic converters (Figure 1).

The main objective of the proposed EM strategy is to manage the distribution of power in such a way as to exploit the performance of the two sources to the best of their ability. The management algorithm for power control is based on a rule-based system, which, in turn, is grounded in the power requested or generated by the two machines (BLDCs), the battery state of charge ( $SOC_{Bat}$ ) and the ultracapacitors state of charge ( $SOC_{UC}$ ).

The scheme of the proposed approach is presented in Figure 14. It can be seen that it depends on:

- The sources characteristics.
- The loads energy needs or generates.

The load power determines the operating mode of two machines, determining whether they use motors or regenerate. If the slope or acceleration is positive, then the load power (2-BLDC powers) is positive, and the vehicle operates in the motor mode; otherwise, it operates in the regenerative braking mode.

$$P_{Sour} = P_{Bat,ref} + P_{UC,ref} \quad (19)$$

$$P_{Sour} = P_{DC,ref}; \quad (P_{Load} \text{ is perturbation}) \quad (20)$$

The reference powers of batteries and UCs can be generated according to the principle described in Figure 15. In order to limit the battery current dynamics, the DC power reference passes through a low-pass filter (LPF) to form the  $i_{Bat,ref}$ . The difference between the DC bus reference power and the battery reference power is used to determine  $P_{ref,UC}$ , which is intended for UCs.

Considering the characteristics of batteries and supercapacitors, their SOC must be taken into consideration when developing references. A switch, controlled by a function of the SOC and the reference coming from the PI correctors, makes it possible to deactivate the batteries or the UCs by assigning 0, respectively, to  $P_{Bat,ref}$  or  $P_U$ .

The flowchart (Figure 16) depicts a rule-based power management strategy that has been proposed (EM). It aims to optimally distribute power between a battery, UC and the load (EV). Based on factors like the power requested by the motor BLDCs, the state of charge of the batteries ( $SOC_{sBat}$ ) and the ultracapacitors state of charge ( $SOC_{UC}$ ), the flowchart determines the power references ( $P_{DC,ref}$  and  $P_{UC,ref}$ ) and potentially triggers the stopping and

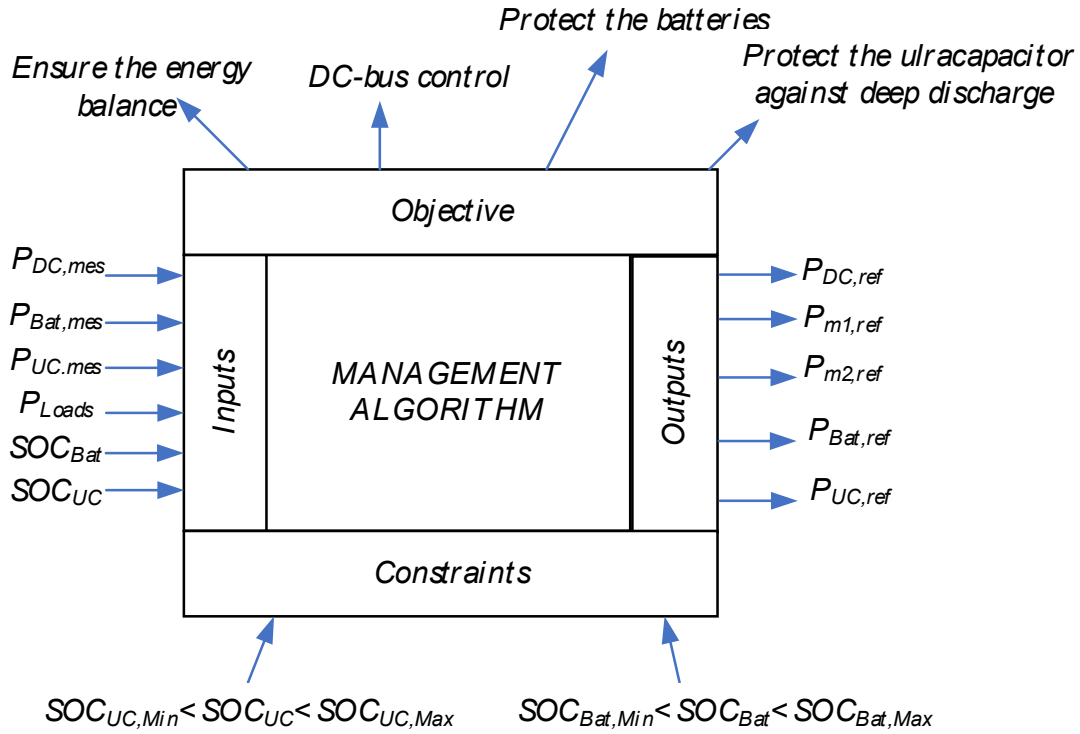


Figure 14. Planning of the proposed sizing algorithm. UC, ultracapacitor.

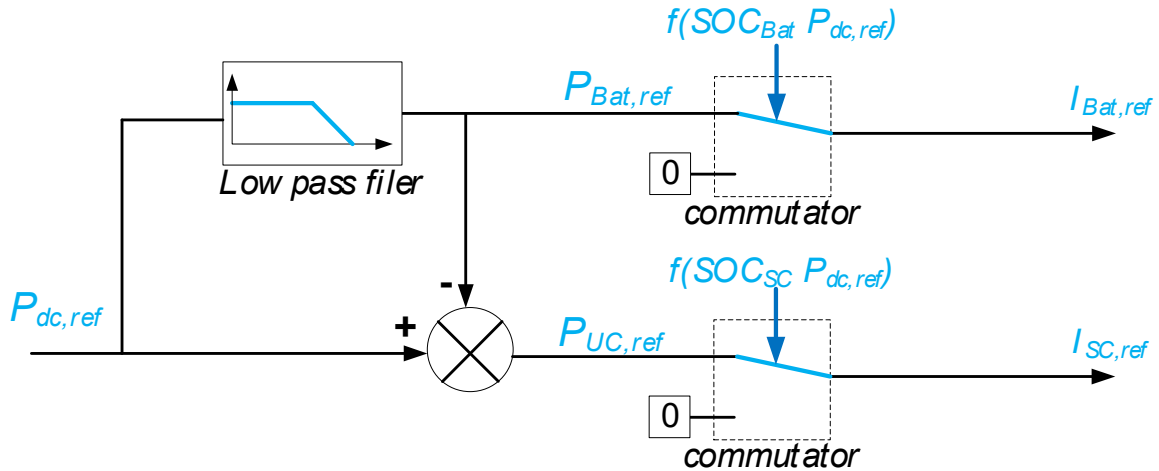
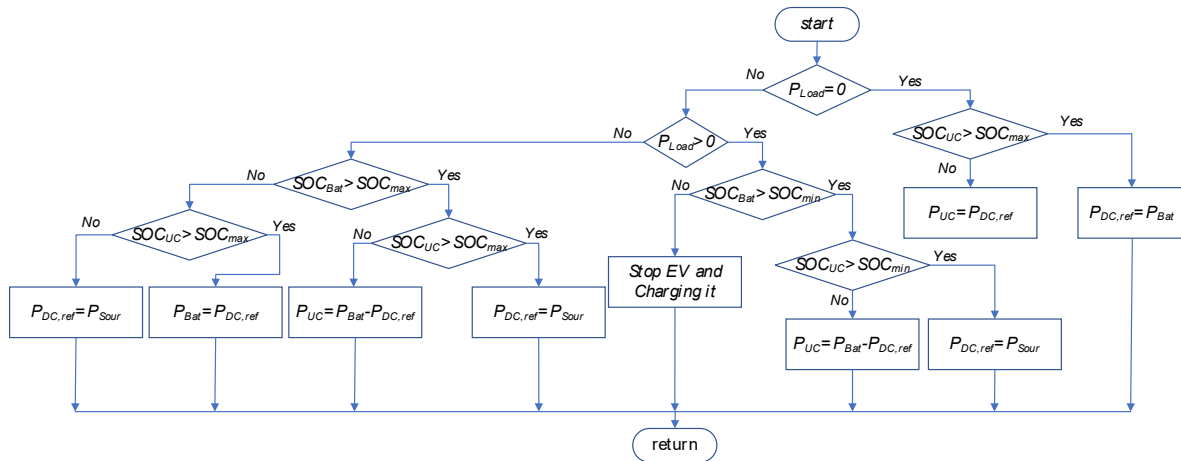


Figure 15. Power references for storage units.



**Figure 16.** Flowchart of the proposed EM method. EM, energy management; EV, electric vehicle.

charging of the EV. This approach ensures that the system leverages the strengths of both the battery and UC to optimise performance.

## 4. Simulation Results and Interpretation

To validate the control and performance of the EM strategy, simulations of the EV systems were implemented using the MATLAB/SimPowerSystems software. The design of the electric powertrain considered the physical attributes outlined in Table 1 and Table 2.

The system considered in the present study consists of two BLDCs with a nominal power of 35 kW, a set of lead batteries  $C_b = 80$  Ah and a set of UCs ( $C_{uc} = 30$  F). The other parameters of the simulation are shown in Table 3.

The common reference speed, as set by the accelerator pedal command, passes through four phases: startup (no speed), acceleration, constant speed operation and deceleration.

In the first stage, the EV starts up, where there is no speed. In this case, the set of battery charges the UCs, This is explained by Figure 17(a–d). After this stage, at 4.8 s the car will start accelerating (second stage) at an initial velocity of 0 Km/h to 30 Km/h. As demonstrated in Figure 17(a), the vehicle's speed development exhibits an excellent time-domain approximation to the required speed. With minor fluctuations, the vehicle nearly precisely matches the speed target.

**Table 1.** Motor drive system parameters.

Parameters	Value
Rated speed	2,500 rpm
Rated power	35 kW
Rated voltage	500 V
Rated torque	135 N.m
Moment of Inertia, J	45e-4 Kg/m <sup>2</sup>
Friction factor	1e-7
Poles number	2
Torque constant	2.62 N.m/A
Efficiency	94.3%

**Table 2** Parameters of the vehicle body.

Parameters	Value	Parameters	Value
Masse of vehicle 'M (kg)'	800	Vehicle frontal area 'Af(m <sup>2</sup> )'	2.5
Transmission ratio 'l'	3.5	Air density 'ρ(kg/m <sup>3</sup> )'	1.28
Aerodynamic drag coefficient 'Cd'	0.32	Wheel radius 'R(m)'	0.33
Tire rolling resistance coefficient 'μ'	0.0015	Earth gravity 'g/m/s <sup>2</sup> '	9.81

**Table 3.** Simulation parameters.

	Storage converters	BLDC
Converter topology	Buck & boost bidirectional converter	Hysteresis inverter
Control technique	Two cascade PI controllers	PI controllers
Control parameters (kp, ki)	Current_Bat: (40, 2,000) Current_UC: (15, 1,000)	Speed: (0.005, 0.1722)
Sample times: System: (discrete, Ts = 5e-6s)	Controllers: Tc, Bat, SC = 5e-5s	Controllers: Tc, ω = 5e-5s.

BLDC, brushless DC motor; UCs, ultracapacitors.

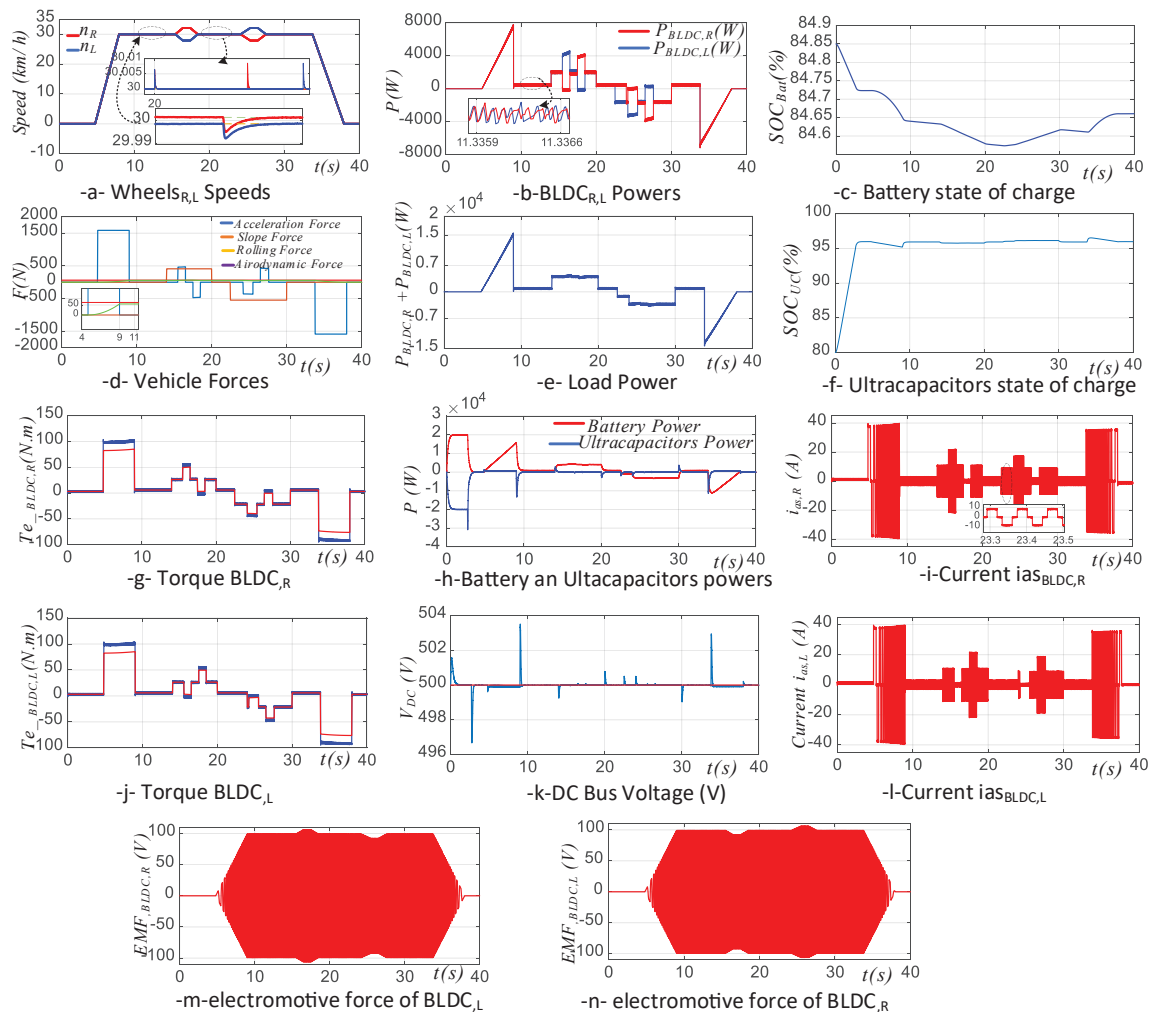


**Figure 17.** Simulation results of an EV. (a) Vehicle speed. (b) BLDC motor powers. (c) Battery state of charge. (g) Torque BLDC, right. (h) Battery and UCs powers. (i) Current  $i_{as}$  BLDC, right. (j) Torque BLDC, left. (k) DC Bus Voltage. (l) Current  $i_{as}$  BLDC, left. (m) electromotive force of BLDC, left. (n) Electromotive force of BLDC, right.

Battery and UC measurements are shown in Figure 17(c,d). In the first case, when the vehicle is stopped, the  $SOC_{UC}$  is  $<95\%$  (see figure 17(f)) since strong acceleration is necessary while the batteries charge the UCs. At  $t = 4.8$  s, the battery-supplied power during acceleration reaches 8 kW but is not able to reach the reference power. An LPF is applied to the charging power, and the UCs start to help the battery by providing extra power as shown in Figure 17(h). This power value does not induce any electrical constraints on the battery. At  $t = 8$  s, the vehicle slightly exceeds the set-point speed with an overshoot, then slows to its reference speed, enabling the supercapacitor and battery to charge dynamics.

After 8 s, the vehicle enters the third stage where the EV is driven at a reference speed fixed at 30 km/h. At 14 s, the car encounters resistance uphill with a gradient of 2%; the torque applied to counter this resistance increases. Consequently, the vehicle quickly regains its desired speed. The battery is gradually asked to provide more power to the load. A LPF is used to smoothen out the load power demand (Figure 17-e), preventing sudden changes from reaching the supercapacitors. Meanwhile, two DC-DC converters operate in the boost mode to increase the voltage to the required level. About 1.5 s later, the vehicle (VE) undergoes a right turn with an angle ( $\alpha$ ) of  $14^\circ$ . The differential immediately influences the two engines by reducing the speed of the right driving wheel (associated with the BLDCR), which is on the inside of the bend, unlike the one located on the outside. When the speed of the right wheel decreases in accordance with its new reference, the torque and current tend to change due to the sudden change in the speed step. This is explained by Figure 17(g),(j),(i) and (l). At the exit of the bend (at  $t = 17.5$  s), the driver gives the opposite steering angle of the steering wheels and differential acts in the same way to make the speed difference zero.

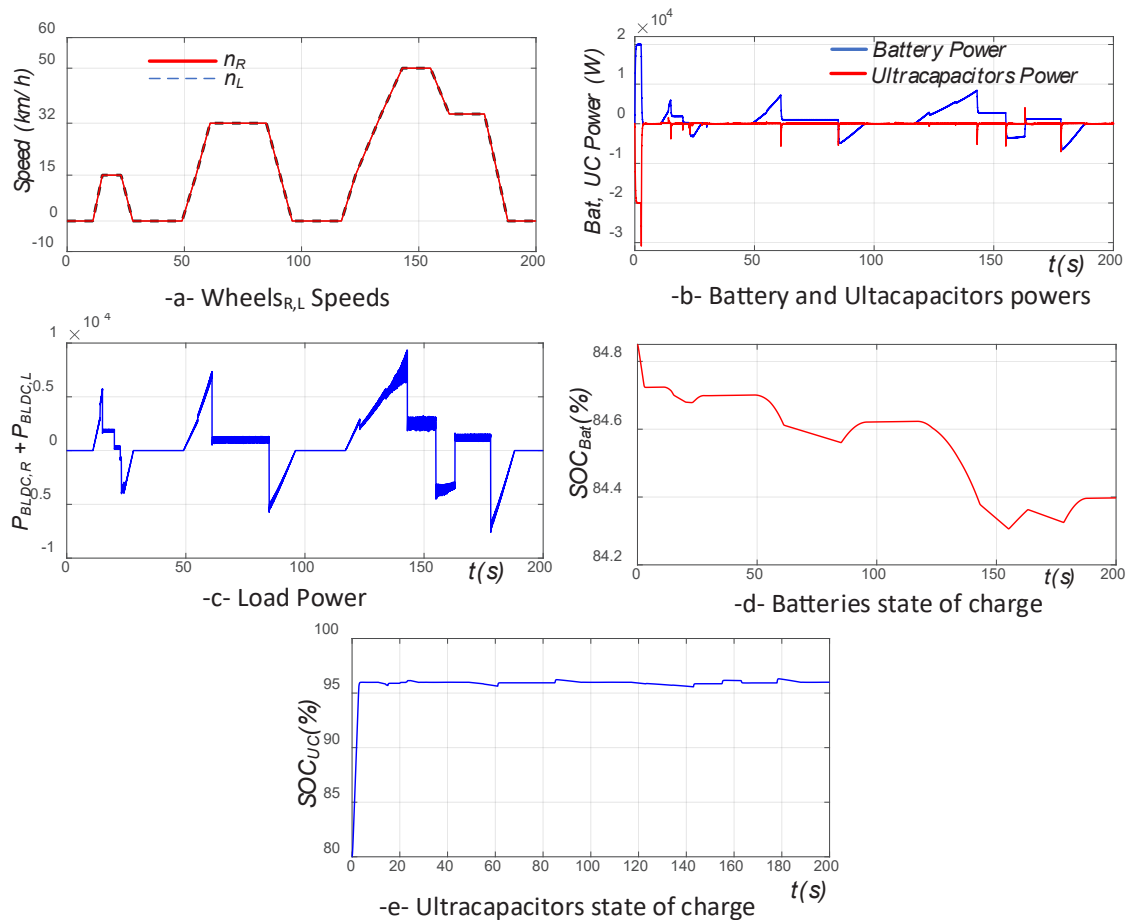


**Figure 18.** Simulation results of an urban drive cycle, ECE-15. (a) Wheels<sub>R,L</sub> Speeds. (b) Batteries and Ultracapacitors powers. (c) Load Power. (d) Batteries state of charge. (e) Ultracapacitors state of charge

At 22.4 s, the vehicle encounters a descent with a 4% slope, causing the load torque to turn negative. This shift to negative load torque (Figure 17- activates regenerative braking, reversing the power flow through the motors. The supercapacitors adapt instantaneously to the load's demands, absorbing current surges as instructed by the EMS, simultaneously converting the EV's kinetic energy into electrical energy that is stored in the battery. In this phase, the vehicle makes a left turn for 1.5 s at a speed of 30 km/h. The drive wheels travel different paths; they rotate in the same direction at different speeds. Upon reaching the end of the downhill section at 30 s, the  $SOC_{UC} > 95\%$ , and the battery assumes sole responsibility for powering the motors.

At  $t = 34$  s, the EV starts to decelerate until it stops (fourth phase). The wheels of the EV drive the BLDC motors, causing them to act as generators. The load power is allocated between the battery and supercapacitor in a way that complies with the principle of energy conservation, with the battery playing the primary role in providing energy.

During the operating cycle, the voltage is illustrated in Figure 17(k). The voltage is maintained at its reference value ( $V_{DC}^* = 500$  V) with permissible variations ( $\pm 1$  V). As expected, there is effective regulation of the DC bus voltage due to the control of the bidirectional chopper.

The simulation utilises the standard driving schedule ECE-15, as illustrated in Figure 18. The speed, power sharing and SOC are presented.

The battery supplies the EV with the required average power and receives energy during braking. Ultracapacitors (UCs) provide supplementary assistance during the acceleration and deceleration phases. Moreover, when the  $SOC_{UC}$  state of charge falls below the minimum threshold, they draw energy from the battery to maintain a minimum energy level, thereby assisting the battery during subsequent acceleration and braking phases.

## 5. Conclusion

In this paper, we proposed and analysed a novel EM and control strategy for EVs. This strategy dynamically distributes DC bus voltage regulation between the battery and UCs based on load requirements, leading to enhanced energy efficiency. Our primary objective is two-fold: maximising vehicle range through efficient energy recovery during deceleration and downhill phases, and extending battery lifespan by integrating UCs to handle transient currents. While the UCs manage short-term power fluctuations, the battery, with its slower time constant, provides the long-term energy needs. This distribution of power demands can be further optimised depending on desired performance characteristics. Our simulation results demonstrate that the proposed EMS effectively maintains a high SOC in the UCs, leading to improved overall EM and increased driving range for EVs.

## References

- AC, R. and Reddy, V. S. (2022). Bidirectional DC-DC Converter Circuits and Smart Control Algorithms: A Review. *Journal of Electrical Systems and Inf Technol*, 9, p. 6. doi: 10.1186/s43067-022-00048-z
- Babu, T. S., Vasudevan, K. R., Ramachandaramurthy, V. K., Sani, S. B., Chemud, S. and Lajim, R. M. (2020). A Comprehensive Review of Hybrid Energy Storage Systems: Converter Topologies, Control Strategies and Future Prospects. *IEEE Access*, 8, pp. 148702–148721. doi: 10.1109/ACCESS.2020.3015919
- Barré, A., Benjamin, D., Grolleau, S., Gérard, M., Suard, F. and Riu, D. (2013). A Review on Lithium-ion Battery Ageing Mechanisms and Estimations. *Journal of Power Sources*, 241, pp. 680–689. doi: 10.1016/j.jpowsour.2013.05.040
- Chhlonh, C., Kim, B., Chrin, P., Am, S. and Seng, T. (2021). Four in-wheel BLDC motors speed control in EV based on hybrid fuzzy-PI controller visual on GUI. In: *IEEE, International Symposium on Electrical and Electronics Engineering (ISEE)*. Ho Chi Minh, Vietnam, pp. 166–171.
- Chojowski, M. (2018). Simulation Analysis of Extended Kalman Filter Applied for Estimating Position and Speed of a Brushless DC Motor. *Power Electronics and Drives*, 3(38), pp. 145–155. doi: 10.2478/pead-2018-0008
- He, Y., Chowdhury, M., Pisu, P. and Ma, Y. (2012). An Energy Optimization Strategy for Power-Split Drivetrain Plug-in Hybrid Electric Vehicles. *Transportation Research Part C: Emerging Technologies*, 22, pp. 29–41. doi: 10.1016/j.trc.2011.11.008

- Itania, K. and De Bernardinis, A. (2022). Management of the energy storage hybridization in electric vehicles. In: *Encyclopedia of Electrical and Electronic Power Engineering*. pp. 542–562.
- Jing, W., Lai, C. H., Wallace Wong, S. H. and Dennis Wong, M. L. (2017). Battery-Supercapacitor Hybrid Energy Storage System in Standalone DC Microgrids: A Review. *IET Renewable Power Generation*, 11(4), pp. 461–469.
- Kamrul, H. M., Mahmud, M., Ahasan Habib, A. K. M., Motakabber, S. M. A. and Islam, S. (2021). Review of Electric Vehicle Energy Storage and Management System: Standards, Issues, and Challenges. *Journal of Energy Storage*, 41, p. 102940. doi: 10.1016/j.est.2021.102940
- Kouchachvili, L., Yaïci, W. and Entchev, E. (2018). Hybrid Battery/Supercapacitor Energy Storage System for the Electric Vehicles. *Journal of Power Sources*, 374, pp. 237–248. doi: 10.1016/j.jpowsour.2017.11.040
- Kuperman, A. and Aharon, I. (2011). Battery–Ultracapacitor Hybrids for Pulsed Current Loads: A Review. *Renewable and Sustainable Energy Reviews*, 15(2), pp. 981–992. doi: 10.1016/j.rser.2010.11.010
- Lahyani, A., Abdelhedi, R., Ammari, A. C., Sari, A. and Venet, P. (2020). Reinforcement learning based adaptive power sharing of battery/supercapacitors hybrid storage in electric vehicles. In: *Energy Sources, Part A: Recovery, Utilization, and Environmental Effects*. pp. 7914–7933.
- Lemian, D. and Bode, F. (2022). Battery-Supercapacitor Energy Storage Systems for Electrical. *Energies*, 15(15), p. 5683. doi: 10.3390/en15155683
- Li, Z., Khajepour, A. and Jinchun, S. (2019). A Comprehensive Review of the Key Technologies for Pure Electric. *Energy*, 182, pp. 824–839. doi: 10.1016/j.energy.2019.06.077
- Listwan, J. J. and Oleszczyszyn, P. (2023). Analysis of the Drive of the Electric Vehicle with Six-Phase Induction Motor. *Power Electronics and Drives*, 8(43), pp. 252–274. doi: 10.2478/pead-2023-0017
- Ma, N., Yang, D., Riaz, S., Wang, L. and Wang, K. (2023). Aging Mechanism and Models of Supercapacitors: A Review. *Technologies*, 11(2), p. 38. doi: 10.3390/technologies11020038
- Ming, T., Deng, W., Wu, J. and Zhang, Q. (2014). A hierarchical energy management strategy for battery-supercapacitor hybrid energy storage system of electric vehicle. In: *2014 IEEE Conference and Expo Transportation Electrification Asia-Pacific*. Beijing, China, pp. 1–5.
- Paire, D., Simões, M. G., Lagorse, J. and Miraoui, A. (2010). A real-time sharing reference voltage for hybrid generation power system. In: *IEEE Industry Applications Society Annual Meeting*. Houston, TX, USA, pp. 1–8.
- Rimpas, D., Kaminaris, S. D., Aldarraj, I., Piromalis, D., Vokas, G., Papageorgas, P. G. and Tsaramiris, G. (2022). Energy Management and Storage Systems on Electric Vehicles: A Comprehensive Review. *Materials Today: Proceedings*, 61, pp. 813–819. doi: 10.1016/j.matpr.2021.08.352
- Salkuti, S. R. (2023). Advanced Technologies for Energy Storage and Electric Vehicles. *Energies*, 16(5), p. 2312. doi: 10.3390/en16052312
- Sandrini, G., Chindamo, D. and Gadola, M. (2022). Regenerative Braking Logic That Maximizes Energy Recovery Ensuring the Vehicle Stability. *Energies*, 15, p. 5846. doi: 10.3390/en15165846
- Sankarkumar, R. S. and Natarajan, R. (2020). Energy management techniques and topologies suitable for hybrid energy storage system powered electric vehicles: An overview. *International Transactions on Electrical Energy Systems*, 31(4). e12819. doi: 10.1002/2050-7038.12819
- Sen, H., Mingyang, L. and Xueqing, W. (2023). Control of BLDC Motor Drive with Single Hall Sensor Considering Angle Compensation. *Power Electronics and Drives*, 8(43), pp. 299–309. doi: 10.2478/pead-2023-0019
- Shen, J. and Khaligh, A. (2015). A Supervisory Energy Management Control Strategy in a Battery/ Ultracapacitor Hybrid Energy Storage System. *IEEE Transactions on Transportation Electrification*, 1(3), pp. 223–231. doi: 10.1109/TTE.2015.2464690
- Sun, X., Li, Z., Wang, X. and Chengjiang, L. (2019). Technology Development of Electric Vehicles: A Review. *Energies*, 13(1), p. 90. doi: 10.3390/en13010090
- Venugopal, P. V. T. and Reka, S. (2023). State of Charge Estimation of Lithium Batteries in Electric Vehicles Using IndRNN. *IETE Journal of Research*, 69(5), pp. 2886–2896. doi: 10.1080/03772063.2021.1906770
- Vodovozov, V., Raud, Z. and Petlenkov, E. (2021). Review on Braking Energy Management in Electric Vehicles. *Energies*, 14(15), p. 4477. doi: 10.3390/en14154477
- Wu, X., Yang, L. and Xu, M. (2014). Speed following control for differential steering of 4WID electric vehicle. In: *40th Annual Conference of the IEEE Industrial Electronics Society*. Dallas, TX, USA, pp. 3054–3059.
- Yahya, A. O. M. and Ould Mahmoud, A. K. (2007). Modélisation d'un système de stockage intégré dans un système hybride (PV/ Eolien/ Diesel).

- Revue des Energies Renouvelables*, 10(2), pp. 205–214. NODOI
- Yuan, H.-B., Zou, W.-J., Jung, S. and Kim, Y.-B. (2022). A Real-Time Rule-Based Energy Management Strategy With Multi-Objective Optimization for a Fuel Cell Hybrid Electric Vehicle. *IEEE Access*, 10, pp. 102618–102628. doi: 10.1109/ACCESS.2022.3208365
- Zebiri, F., Abdelhalim, K., Lazhar, R. and Ali, C. (2016). Analysis and Design of Photovoltaic Pumping System based on Nonlinear Speed Controller. *Journal of Power Technologies*, 96, pp. 40–48.
- Zebiri, F., Choudar, A., Kessal, A. and Rahmani, L. (2022). Non-conventional implementation of the speed controller applied to a brushless DC motor with trapezoidal back EMF. In: *19th International Multi-Conference on Systems, Signals & Devices (SSD)*. Sétif, Algeria, pp. 1865–1870.
- Zhang, L., Hu, X., Wang, Z., Sun, F. and Dorrell, D. G. (2017). A Review of Supercapacitor Modeling, Estimation, and Applications: A Control/Management Perspective. *Renewable and Sustainable Energy Reviews*, 81, pp. 1868–1878. doi: 10.1016/j.rser.2017.05.283